



Comparing amyloid- β plaque burden with antemortem PiB PET in autosomal dominant and late-onset Alzheimer disease

Charles D. Chen¹ · Nelly Joseph-Mathurin¹ · Namita Sinha^{2,3} · Aihong Zhou⁴ · Yan Li⁵ · Karl Friedrichsen⁶ · Austin McCullough¹ · Erin E. Franklin² · Russ Hornbeck¹ · Brian Gordon¹ · Vijay Sharma¹ · Carlos Cruchaga⁷ · Alison Goate⁸ · Celeste Karch⁷ · Eric McDade⁵ · Chengjie Xiong⁵ · Randall J. Bateman⁵ · Bernardino Ghetti⁹ · John M. Ringman¹⁰ · Jasmeer Chhatwal¹¹ · Colin L. Masters¹² · Catriona McLean¹³ · Tammaryn Lashley^{14,15} · Yi Su^{16,17} · Robert Koeppe¹⁸ · Clifford Jack¹⁹ · William E. Klunk²⁰ · John C. Morris⁵ · Richard J. Perrin^{2,5} · Nigel J. Cairns^{2,5,21} · Tammie L. S. Benzinger¹

Received: 12 March 2021 / Revised: 29 June 2021 / Accepted: 1 July 2021 / Published online: 28 July 2021
© The Author(s), under exclusive licence to Springer-Verlag GmbH Germany, part of Springer Nature 2021

Abstract

Pittsburgh compound B (PiB) radiotracer for positron emission tomography (PET) imaging can bind to different types of amyloid- β plaques and blood vessels (cerebral amyloid angiopathy). However, the relative contributions of different plaque subtypes (diffuse versus cored/compact) to in vivo PiB PET signal on a region-by-region basis are incompletely understood. Of particular interest is whether the same staging schemes for summarizing amyloid- β burden are appropriate for both late-onset and autosomal dominant forms of Alzheimer disease (LOAD and ADAD). Here, we compared antemortem PiB PET with follow-up postmortem estimation of amyloid- β burden using stereologic methods to estimate the relative area fraction of diffuse and cored/compact amyloid- β plaques across 16 brain regions in 15 individuals with ADAD and 14 individuals with LOAD. In ADAD, we found that PiB PET correlated with diffuse plaques in the frontal, parietal, temporal, and striatal regions commonly used to summarize amyloid- β burden in PiB PET, and correlated with both diffuse and cored/compact plaques in the occipital lobe and parahippocampal gyrus. In LOAD, we found that PiB PET correlated with both diffuse and cored/compact plaques in the anterior cingulate, frontal lobe (middle frontal gyrus), and parietal lobe, and showed additional correlations with diffuse plaque in the amygdala and occipital lobe, and with cored/compact plaque in the temporal lobe. Thus, commonly used PiB PET summary regions predominantly reflect diffuse plaque burden in ADAD and a mixture of diffuse and cored/compact plaque burden in LOAD. In direct comparisons of ADAD and LOAD, postmortem stereology identified much greater mean amyloid- β plaque burdens in ADAD versus LOAD across almost all brain regions studied. However, standard PiB PET did not recapitulate these stereologic findings, likely due to non-trivial amyloid- β plaque burdens in ADAD within the cerebellum and brainstem—commonly used reference regions in PiB PET. Our findings suggest that PiB PET summary regions correlate with amyloid- β plaque burden in both ADAD and LOAD; however, they might not be reliable in direct comparisons of regional amyloid- β plaque burden between the two forms of AD.

Keywords Alzheimer disease · Amyloid- β plaques · PiB PET · Stereology

Introduction

Pittsburgh compound B (PiB) positron emission tomography (PET) is a powerful diagnostic tool that enables in vivo imaging of insoluble amyloid- β throughout the human brain at near-millimeter resolution [37]. This offers an opportunity to detect and monitor changes in amyloid- β plaque deposition during the course of Alzheimer disease (AD) clinical trials. However, some important characteristics of PiB, as it is applied in vivo, remain incompletely understood.

Nelly Joseph-Mathurin, Namita Sinha and Aihong Zhou have contributed equally to this work.

Nigel J. Cairns and Tammie L.S. Benzinger are co-senior authors.

✉ Tammie L. S. Benzinger
benzingert@wustl.edu

Extended author information available on the last page of the article

Although PiB is known to bind to amyloid- β peptides associated with both diffuse and amyloid- β cored/compact plaques [46], the relative contributions of these plaque subtypes to in vivo PiB PET signal on a region-by-region basis remain incompletely understood. The distinction is of interest from a clinicopathological perspective, as cored/compact plaques are more likely than their diffuse counterparts to be neuritic [16, 4, 54]. Nonetheless, diffuse plaques are associated with deleterious effects on cognitive performance and are unlikely to be benign [58]. Additionally, as AD clinical trials involve both late-onset AD (LOAD) and autosomal dominant AD (ADAD) populations, there is a need to understand whether the staging schemes for summarizing amyloid- β burden in the former are appropriate for investigating the severity of β -amyloidosis in the latter. In contrast to individuals with LOAD, those with ADAD carry a mutation in one of three genes—*APP*, *PSEN1*, or *PSEN2*—and develop AD with a relatively predictable time of clinical onset. This defining characteristic of ADAD allows investigators to assess the extent to which candidate drugs are preventing or delaying the onset of AD dementia, but this underlying difference in disease etiology may also lead to differences in the characteristics of β -amyloidosis between LOAD and ADAD populations [1, 60].

Commonly, postmortem staging of amyloid- β deposition in AD involves assessment of Thal phase [72] and the Consortium to Establish a Registry for Alzheimer disease (CERAD) neuritic plaque score [50], which have recently been incorporated, along with Braak neurofibrillary tangle (NFT) stage [4], into the ABC score [28]. Although very useful for some purposes, these systems only describe the general anatomic pattern of amyloid- β plaque deposition within the central nervous system (Thal phase) and the semi-quantitative maximal density of neuritic plaques within a prescribed, limited set of cortical regions (CERAD). For antemortem staging of amyloid- β deposition in AD, a volume of interest comprised of frontal, parietal, temporal, and striatal regions is typically constructed to focus on brain regions of greater relevance to AD disease pathology [38, 67]; however, these regions were derived by comparing groups of healthy individuals and individuals with LOAD. Thus, from both neuropathologic and imaging perspectives, it is unclear whether these staging schemes for amyloid- β burden are equally applicable to both ADAD and LOAD.

Therefore, to investigate more fully the qualities of β -amyloidosis in these two forms of AD, we examined two cohorts, representing ADAD and LOAD, using antemortem PiB PET imaging and unbiased stereologic methods to quantify postmortem amyloid- β burden contributed by diffuse and cored/compact plaques in 16 brain regions of interest, including seven summary regions typically of interest in PiB PET imaging of AD (frontal, parietal, and temporal lobes, anterior and posterior regions of

the cingulate gyrus, caudate, and putamen), seven other regions typically of interest for the evaluation of various other AD and non-AD pathologic features (occipital lobe, amygdala, hippocampus, parahippocampal gyrus, entorhinal cortex, globus pallidus, and thalamus), and two reference regions typically of interest in PiB PET imaging of AD (cerebellum and brainstem). We then compared these findings to corresponding antemortem PiB PET, to determine whether the relationship between histologic and PET assessments of amyloid- β pathology is influenced by plaque type, anatomic region, and form of AD. This study provides insights into the extent to which plaque subtypes are represented in typical PiB PET neuroimaging and the extent to which differences in amyloid- β plaque burden between ADAD and LOAD are represented in typical PiB PET. Thus, this study informs how PiB PET might best be applied to evaluate ADAD progression in AD clinical trials, and how amyloid- β clearance might be appropriately monitored in anti-amyloid- β drug trials.

Materials and methods

Cohort demographics

Participants selected for this histological/radiological comparison study were either enrolled in the Dominantly Inherited Alzheimer Network Observational Study (DIAN-Obs, $n = 14$) or in longitudinal observational studies of the Charles F. and Joanne Knight Alzheimer Disease Research Center (Knight ADRC, $n = 15$). One participant was enrolled in studies of the Knight ADRC, but had an ADAD mutation; this individual was grouped with participants from the DIAN-Obs to form the ADAD cohort ($n = 15$), and the remaining participants from the Knight ADRC formed the LOAD cohort ($n = 14$) in the current study (Table 1). All participants met the inclusion criteria, having undergone PiB PET prior to death, and having *high* AD neuropathologic change (ADNC) upon subsequent postmortem examination [51]. Cohort demographics are reported in Table 1.

To address other questions about PiB PET amyloid staging, a separate extended imaging cohort of 317 DIAN-Obs participants and 734 Knight ADRC participants was selected. These participants met the inclusion criteria of having had a clinical and cognitive assessment within 18 months of a PiB PET scan. Extended imaging cohort demographics are reported in Table 3. Protocols for the study have received prior approval by the local Institutional Review Board (IRB) or Ethics Committee of each DIAN site, and by the Washington University IRB for the Knight ADRC. Participants or their caregivers provided written informed consent.

Table 1 Cohort demographics

	Family mutation	APOE	Sex	MMSE	CDR	Clinical cause of death	CDR at death	Age at death	Imaging-autopsy interval (years)	Thal phase	Braak stage	CERAD score	CAA	Final Dx 1	Final Dx 2–4
ADAD															
1	<i>PSEN1</i>	44	M	21	1	Aspiration, pneumonia, AD	3	40–50	0.68	5	6	3	1	ADNC	Glrioblastoma
2	<i>PSEN1</i>	23	F	16	1	Probable pneumonia	3	30–40	1.1	5	6	3	1	ADNC	
3	<i>PSEN1</i>	33	M	9	3	Inanition	3	40–50	1	5	6	3	2	ADNC	DLB (neocortical), SVD; CAA (moderate-severe), Art. (mild)
4	<i>PSEN1</i>	34	F	21	1	AD	3	40–50	3.3	5	6	3	3	ADNC	DLB
5	<i>PSEN1</i>	23	F	12	2	Probable pneumonia	3	40–50	2.3	5	6	3	2	ADNC	
6	<i>PSEN1</i>	33	M	10	1	AD, inanition	3	40–50	1.8	5	6	3	1	ADNC	DLB
7	<i>PSEN1</i>	33	M	13	2	AD, inanition	3	50–60	1.3	5	6	3	1	ADNC	ALB
8	<i>PSEN1</i>	23	F	8	2	Respiratory failure, cardiac arrest, AD	3	40–50	1.5	5	6	3	1	ADNC	MH (BG)
9	<i>PSEN1</i>	34	F	21	0.5	AD	3	30–40	2.5	5	6	3	3	ADNC	
10	<i>PSEN1</i>	33	M	0	3	Heart attack, Inanition	3	60–70	4	5	6	3	1	ADNC	ALB
11	<i>PSEN1</i>	34	F	8	3	AD, inanition	3	40–50	2.3	5	6	3	3	ADNC	ALB
12	<i>PSEN1</i>	33	M	15	1	Aspiration, inanition	3	50–60	2	5	6	3	3	ADNC	CAA
13	<i>PSEN1</i>	33	M	19	1	Brain hemorrhage, inanition	3	50–60	3.4	5	6	3	2	ADNC	ALB
14	<i>APP</i>	44	M	21	2	Pneumonia, inanition	3	60–70	5.6	5	6	3	3	ADNC	ALB
15	<i>PSEN1</i>	33	M	27	0.5	AD	3	30–40	3.3	5	6	3	3	ADNC	

Table 1 (continued)

	Family mutation	APOE	Sex	MMSE	CDR	Clinical cause of death	CDR at death	Age at death	Imaging-autopsy interval (years)	Thal phase	Braak stage	CERAD score	CAA	Final Dx 1	Final Dx 2–4
Mean (SD)				15 (7)	1.6 (0.9)		3 (0)	47 (9)	2.4 (1.3)	5 (0)	6 (0)	3 (0)	2 (0.9)		
LOAD															
1	34	M	M	30	0.5	UTI, diabetes mellitus, AD con-tributing	2	80–90	3.7	5	5	3	1	ADNC	SVD: Art. (moderate), LVD: Art. (moderate)
2	33	M	M	21	1	Lymphoma	2	60–70	3.9	5	6	3	1	ADNC	
3	34	F	F	20	1	AD	3	80–90	3.8	5	5	3	1	ADNC	
4	34	F	F	26	0.5	Inanition	3	70–80	3.9	5	5	3	3	ADNC	
5	34	M	M	12	2	AD	3	70–80	4.7	5	5	3	1	ADNC	
6	34	F	F	28	0	AD	3	80–90	4.8	5	4	3	1	ADNC	
7	34	M	M	25	0.5	DLB, UTI, dehydration	3	70–80	3.7	5	5	3	1	ADNC	
8	33	M	M	22	1		1	80–90	0.3	5	5	3	1	ADNC	
9	34	M	M	26	0.5	Inanition	3	80–90	3.4	4	5	3	1	ADNC	
10	34	F	F	25	0.5	Inanition	3	90–100	8.4	4	6	3	2	ADNC	Infarcts (BG, Th)
11	34	M	M	26	0.5	Inanition	3	90–100	9.6	5	5	3	3	ADNC	ALB, TDP-43 (MTL)
12	34	M	M	23	0.5	Inanition	3	70–80	4.2	5	5	3	1	ADNC	
13	33	F	F	25	0.5		2	90–100	6.1	5	5	3	2	ADNC	Infarcts (PL, FL), micro-infarct (FL)
14	33	M	M	23	0.5	AD	3	70–80	4.9	5	6	3	1	ADNC	DLB (olfactory), SVD: Art. (moderate), SVD: CAA (mild)
Mean (SD)				24 (4)	0.7 (0.5)		2.6 (0.6)	83 (9)	4.7 (2.2)	5.1 (0.5)	3 (0)	3 (0)	1.4 (0.8)		

Age at death is reported as an age range to protect the identities of the study participants. Exact ADAD mutations of the *PSEN1* gene are presented in Online Resource 2 in the interests of better understanding the clinicopathologic variability in this population, but are not linked to the individual-level demographics in this table to protect the identities of the study participants

ADNC Alzheimer disease neuropathologic change, ALB amygdala Lewy bodies, Art. arteriosclerosis, BG basal ganglia, CAA cerebral amyloid angiopathy, DLB dementia with Lewy bodies, Dx diagnosis, FL frontal lobe, LVD large vessel disease, MH microhemorrhage, MTL medial temporal lobe, PL parietal lobe, PL microhemorrhage, SAH subarachnoid hemorrhage, SD standard deviation, SVD small vessel disease, Th thalamus, UTI urinary tract infection

Postmortem neuropathology

Neuropathologic assessment of cases included a systematic evaluation of histologic slides representing 16 areas from the left hemisphere by experienced neuropathologists (authors R.J.P. and N.J.C.) [7]. Following an established protocol, each left hemisphere was sliced after formalin fixation. The supratentorial portion of the cerebral hemisphere was sliced in the coronal plane; the cerebellum, parasagittally; and the brainstem, axially. Sixteen representative brain areas were sampled: the frontal lobe (middle frontal gyrus); temporal lobe (superior and middle temporal gyri); parietal lobe (inferior parietal cortex including the angular gyrus); occipital lobe (including the calcarine sulcus and parastriate cortex); anterior cingulate gyrus (at the level of the genu of the corpus callosum); posterior cingulate gyrus (including precuneus at the level of the splenium); amygdala; hippocampus, parahippocampal gyrus, and entorhinal cortex (at the level of the lateral geniculate nucleus); caudate, putamen, and globus pallidus (at the level of the anterior commissure); thalamus (including subthalamic nucleus); brainstem (midbrain, pons, medulla oblongata); and cerebellum (with the dentate nucleus). Slide-mounted 6- μ m-thick sections of formalin-fixed, paraffin-embedded tissue were stained with hematoxylin and eosin (H&E), with a modified Bielschowsky silver impregnation, and by immunohistochemistry (IHC) using antibodies for amyloid- β (10D5, Eli Lilly, Indianapolis, IN, USA), phosphorylated tau (PHF-1, a gift from Dr. Peter Davies), phosphorylated alpha-synuclein (Cell Applications, San Diego, CA, USA), and phosphorylated TAR DNA binding protein of 43 kDa (TDP-43, Cosmo Bio USA, Carlsbad, CA, USA) to detect the histopathological hallmarks of AD as well as those of frequent comorbid pathologies (including non-AD tauopathies, TDP-43 proteinopathies, and α -synucleinopathies). The Area Fraction Fractionator probe in Stereo Investigator 10 (MBF Bioscience, Williston, VT, USA) was used to assess the burden of diffuse and cored/compact amyloid- β using stereologic methods as implemented in a computerized image analysis system. Plaque area fraction was assessed either in the gray matter of cortical gyri or subcortical nuclei. Diffuse amyloid- β plaques were identified by raters (A.Z. and N.S.) to be irregularly shaped amyloid- β deposits, while cored/compact amyloid- β plaques were identified to be spherically shaped amyloid- β deposits representing a dense central core (surrounded by a less compact halo of amyloid- β oligomers contributing to the diffuse rather than the compact amyloid- β plaque area fraction) [30, 78]. The degree of agreement among raters in assessing diffuse and cored/compact amyloid- β plaque burden was high (Cohen's $\kappa > 0.8$). When assessing amyloid- β plaque area fraction, raters were blinded to any demographic

information regarding the individuals who donated the tissue samples, as well as any information regarding their antemortem PiB PET acquisition.

Antemortem PiB PET imaging

Methods for antemortem PiB PET acquisition, performed in compliance with the DIAN protocol, have been described previously [2, 20]. Briefly, participants received an intravenous injection of approximately 15 mCi of [11 C]PiB radiotracer [81]. PET images were attenuation compensated with the corresponding CT image, and reconstructed using the ordered subset expectation maximization technique. Data from 40 to 70 min post-injection were converted to regional standardized uptake value ratios (SUVRs) with the cerebellar gray matter as the standard reference region, with cerebellar white matter and brainstem evaluated as alternative reference regions in later analyses. Regional SUVRs of interest were defined by FreeSurfer [22] version 5.3 regions best corresponding to the areas sampled for neuropathology in a consensus between an experienced neuropathologist and radiologist (authors R.J.P. and T.L.S.B.) [10]. MR images used for FreeSurfer segmentation were also performed in compliance with the DIAN protocol, as described previously [2, 52]. Briefly, T1-weighted images (1.1 \times 1.1 \times 1.2 mm resolution) were acquired for all DIAN-Obs participants on 3T scanners within 1 year of their PET scan.

Methods for antemortem PiB PET and MRI at the Knight ADRC have been described previously [67, 68]. These methods notably differ from the DIAN protocol in the following manner: PET imaging data from 30 to 60 min post-injection were converted to regional SUVRs (in contrast to the 40–70 min post-injection time window for DIAN) and MR imaging was acquired on either a 1.5 or 3T scanner (in contrast to only 3T scanners for DIAN).

Briefly, brain areas sampled for neuropathologic assessment were matched to FreeSurfer regions on the basis of shared nomenclature and spatial overlap on the left hemisphere (Online Resource 1). All data processing steps were performed using the PET Unified Pipeline [67, 66], a publicly available software developed in house.

Statistical analysis

All statistical analyses were performed in R version 3.5.2 “Eggshell Igloo”. Multiple imputation was used in the ADAD (15 participants) and LOAD (14 participants) cohorts to estimate missing observations due to the occasional unavailability of postmortem tissue samples; specifically, 17 tissue samples in the ADAD cohort (out of a possible 240, yielding 7.1% missingness) and 13 tissue samples in the LOAD cohort (out of a possible 224, yielding 5.8% missingness) were unavailable and subsequently

estimated by multiple imputation by chained equations using the predictive mean matching method and five imputations [6]. Pearson's r was used to measure the linear correlation between regional PiB PET SUVR and diffuse and compact plaque area fractions in ADAD and LOAD cohorts. T -values from Welch two sample t tests were used to determine the extent to which regional PiB PET SUVR and diffuse and compact plaque area fractions differed between ADAD and LOAD cohorts. Area under the receiver-operating characteristic curves (AUCs, interpreted as the probability that a randomly selected ADAD/LOAD individual has a higher regional PiB PET SUVR than a randomly selected non-carrier/young healthy control) were used to determine which regions were most frequently elevated in ADAD/LOAD versus young healthy controls. Hierarchical agglomerative clustering was used to visualize similarities in regional PiB PET SUVR distributions across participants (complete-linkage clustering using a Euclidean distance metric). All test statistics are accompanied by p values adjusted for false discovery rate (FDR) control by the Benjamini–Hochberg procedure. An FDR of $q=0.05$ was chosen for discussion purposes, but all FDR-adjusted p values have been reported for transparency [20].

Results

Cohort demographics

Participants who formed the ADAD cohort in this study ($n=15$) were mostly known *PSEN1* mutation carriers ($n=13$), male ($n=9$), lacking the *APOE4* allele ($n=10$), and died at the average age of 47 from AD with other comorbidities (Table 1). All ADAD participants were Thal phase 5, and Braak NFT stage VI, with “frequent” CERAD neuritic plaque scores.

Participants who formed the LOAD cohort in this study ($n=14$) were mostly male ($n=9$) *APOE4* carriers ($n=10$) who died at the average age of 83 with AD and other comorbidities. LOAD participants were largely Thal phase 5 (with two borderline Thal phase 4/5 cases), Braak NFT stage V ($n=10$), with “frequent” CERAD neuritic plaque scores.

In addition to the age of death, the major difference to note between the ADAD and LOAD cohorts is that the imaging-autopsy interval in the ADAD cohort is on average less than the imaging-autopsy interval in the LOAD cohort (an average of 2.4 years versus an average of 4.7 years) due to procedural differences between DIAN-Obs and Knight ADRC studies. We address the potential impact of this difference in the section “Discussion”.

In the extended imaging cohort, ADAD participants ($n=317$) were mostly *PSEN1* mutation carriers ($n=131$) or non-carriers/young healthy controls ($n=133$), female

($n=182$), and cognitively normal ($n=251$), lacked the *APOE4* allele ($n=222$), and underwent PiB PET at an average age of 38 (Table 3).

LOAD participants ($n=734$) were mostly female ($n=421$) and cognitively normal ($n=615$), lacked the *APOE4* allele ($n=451$), and underwent PiB PET at an average age of 69.

Correlations between PiB PET and stereologic measurements

Regional correlations between PiB PET SUVR and diffuse and compact plaque area fractions in the ADAD and LOAD cohorts are shown in Table 2. In the ADAD cohort, PiB PET SUVR was significantly correlated (FDR-adjusted p value <0.05) with diffuse plaque burden in all PiB PET summary regions except for the putamen, and with both diffuse and cored/compact plaque burden in the occipital lobe and parahippocampal gyrus (reference regions were not assessed in these correlational analyses). In the LOAD cohort, PiB PET SUVR was significantly correlated with both diffuse and cored/compact plaque burdens in the anterior cingulate, frontal lobe, and parietal lobe summary regions, and with cored/compact plaque burden in the temporal lobe summary region. Additionally, PiB PET SUVR was significantly correlated with diffuse plaque burden in the amygdala and occipital lobe (Table 3).

Differences between ADAD and LOAD as measured by PiB PET and stereology

Regional differences in amyloid- β burden (as measured by PiB PET and stereology) between the ADAD and LOAD cohorts are shown in Fig. 1. Diffuse plaque burden was significantly greater in ADAD versus LOAD in all summary regions except for the parietal lobe, and in all other regions, except for the globus pallidus. Cored/compact plaque burden was also greater in ADAD versus LOAD, though only in the cerebellum and brainstem was this difference significant.

In contrast to stereologic measurements, PiB PET SUVRs (when calculated using the cerebellar gray matter as a reference region) showed no significant differences between ADAD versus LOAD in any summary region examined, with the exceptions of the caudate and the putamen. Additionally, PiB PET SUVR was significantly greater in ADAD versus LOAD in the hippocampus, occipital lobe, and thalamus. Alternative reference regions such as the brainstem, cerebellar white matter, and a combined cerebellar gray and white matter region were also investigated (Fig. 2). The brainstem as a reference region yielded results similar to those when cerebellar gray matter was used as a reference region (and additionally showed significant differences in the globus pallidus). When cerebellar white matter was used

Table 2 Regional correlations between [11C]PiB PET SUVRs and plaque area fractions

ADAD	Diffuse plaque			Compact plaque		
	<i>R</i>	<i>SE</i>	<i>p</i>	<i>r</i>	<i>SE</i>	<i>p</i>
Summary regions						
Anterior cingulate	0.81	0.16	0.0018	0.32	0.26	0.45
Caudate	0.62	0.22	0.018	0.066	0.28	0.87
Frontal lobe	0.63	0.19	0.018	0.31	0.26	0.45
Parietal lobe	0.70	0.20	0.012	0.59	0.22	0.15
Posterior cingulate	0.63	0.22	0.018	0.045	0.28	0.87
Putamen	0.34	0.26	0.21	−0.084	0.28	0.87
Temporal lobe	0.60	0.22	0.021	0.31	0.26	0.45
Other regions						
Amygdala	0.43	0.25	0.11	0.58	0.23	0.053
Entorhinal cortex	0.46	0.25	0.081	0.48	0.24	0.10
Globus pallidus	−0.013	0.28	0.96	0.12	0.28	0.79
Hippocampus	0.29	0.27	0.30	0.56	0.23	0.053
Occipital lobe	0.80	0.17	0.00038	0.65	0.21	0.030
Parahippocampal gyrus	0.64	0.21	0.011	0.65	0.21	0.030
Thalamus	0.48	0.24	0.073	0.059	0.28	0.83
LOAD						
Summary regions						
Anterior cingulate	0.82	0.16	0.00098	0.68	0.21	0.018
Caudate	0.36	0.27	0.25	0.087	0.29	0.77
Frontal lobe	0.72	0.20	0.0080	0.81	0.17	0.0028
Parietal lobe	0.83	0.16	0.00098	0.62	0.23	0.030
Posterior cingulate	0.23	0.28	0.43	0.23	0.28	0.61
Putamen	0.52	0.25	0.077	−0.087	0.29	0.77
Temporal lobe	0.54	0.24	0.077	0.68	0.21	0.018
Other regions						
Amygdala	0.71	0.20	0.016	0.34	0.27	0.32
Entorhinal cortex	0.072	0.29	0.81	−0.44	0.26	0.26
Globus pallidus	0.14	0.29	0.81	0.13	0.29	0.77
Hippocampus	0.081	0.29	0.81	−0.059	0.29	0.84
Occipital lobe	0.77	0.18	0.0090	0.39	0.27	0.29
Parahippocampal gyrus	0.49	0.25	0.14	0.59	0.23	0.18
Thalamus	0.50	0.25	0.14	0.48	0.25	0.26

p values are adjusted for FDR control by the Benjamini–Hochberg procedure. Estimates associated with *p* values < 0.05 are indicated in bold

SE standard error

as a reference region, PiB PET SUVRs showed additional significant differences between ADAD versus LOAD in the anterior cingulate, amygdala, entorhinal cortex, globus pallidus, brainstem, and cerebellum. Use of the combined cerebellar gray and white matter reference region mostly recapitulated the significant differences between ADAD versus LOAD as seen with the cerebellar white matter reference region, with the exception of the amygdala and entorhinal cortex. Nonetheless, no reference region assessed in this study revealed significant between-cohort differences in SUVR in the frontal and temporal lobes, posterior cingulate, and parahippocampal gyrus in a manner concordant

with our stereology results. Additionally, the alternative reference regions showed significant between-cohort differences in SUVR in the globus pallidus, which was not seen in stereology.

PiB PET staging in ADAD versus LOAD

Regional distributions of PiB PET SUVRs in ADAD versus LOAD are shown in Fig. 3. Regional AUC analyses showed that ADAD participants frequently demonstrate elevated PiB PET SUVRs compared to non-carriers/young healthy controls across all brain regions, with several medial temporal

Table 3 Extended imaging cohort demographics

		ADAD	LOAD
Number		317	734
Family mutation	<i>PSEN1</i>	131	
	<i>PSEN2</i>	22	
	<i>APP</i>	31	
	Non-carrier	133	
<i>APOE</i>	22	3	3
	23	28	80
	24	12	18
	33	191	368
	34	78	209
	44	5	42
Sex	M	135	313
	F	182	421
Mean baseline MMSE (SD)		28.8 (8.61)	28.7 (1.86)
Baseline CDR	0	251	615
	0.5	43	98
	1	16	21
	2	5	0
	3	2	0
Mean baseline age (SD)		37.7 (10.7)	68.7 (9.49)

lobe regions being the least frequently elevated, namely the amygdala, hippocampus, and entorhinal cortex (Fig. 3a). In contrast, LOAD participants most frequently demonstrate elevated PiB PET SUVRs compared to non-carriers/young healthy controls across several temporal lobe regions, namely the middle temporal, inferior temporal, and fusiform cortices (Fig. 3b). In a hierarchical agglomerative clustering dendrogram of ADAD cases, caudate and putamen PiB PET SUVRs cluster with cortical SUVRs such as those of the occipital lobe, frontal lobe, and the anterior and posterior cingulate (Fig. 3c). In contrast, in LOAD, caudate and putamen SUVRs cluster with medial temporal lobe SUVRs such as those of the parahippocampal gyrus, entorhinal cortex, amygdala, and hippocampus rather than frontal and cingulate cortex SUVRs (Fig. 3d).

Discussion

Evidence suggests that the primary substrate for PiB retention (and likely that of all PET amyloid- β radiotracers) is fibrillar amyloid- β [39]. Fibrillar amyloid- β is present in both diffuse and cored/compact plaques—although the density is probably much greater in the latter [15]. Therefore, in vivo PiB retention cannot distinguish between diffuse and cored/compact deposits of fibrillar amyloid- β . However, the total PiB signal will be primarily driven by the most abundant form of fibrillar amyloid- β , whether in diffuse or cored/

compact plaques. To determine which form of plaque (diffuse or cored/compact) is most associated with the in vivo PiB PET signal, postmortem-to-in vivo correlative studies must be performed. In this study, we compared the correlation of in vivo PiB PET retention with postmortem analyses of diffuse and cored/compact plaques in ADAD and LOAD to determine the major contributor to the in vivo PiB PET signal in these different forms of AD. From correlational analyses, PiB PET SUVRs in AD summary regions appear to reflect predominantly diffuse plaque burden in ADAD, and a mixture of diffuse and cored/compact plaque burden in LOAD. Outside of these summary regions, PiB PET SUVRs seem to correlate with both diffuse and cored/compact plaque burden in the occipital lobe and parahippocampal gyrus in ADAD, and with diffuse plaque burden in the occipital lobe and amygdala in LOAD. These differences suggest that the two forms of AD may require different β -amyloidosis staging schemes to interpret findings from PiB PET. Furthermore, the greater variability of plaque burden observed among ADAD cases additionally suggests that a staging scheme for ADAD might require adjustment for other factors, such as, perhaps, genetic subtype. Nonetheless, some caution is warranted: the presence of cored/compact plaques in several of the aforementioned brain regions is a sign of advanced disease which, in turn, is associated with altered blood flow. Changes in blood flow associated with advanced AD may alter PiB pharmacokinetics and cause nonspecific retention in affected brain areas [3]; such pathophysiological changes may be partly responsible for the above observations.

Postmortem stereologic measurements of diffuse and cored/compact plaque burden are significantly greater in ADAD versus LOAD across the brain, yet standard antemortem PiB PET in the same individuals captured significant differences mostly in subcortical regions (specifically the caudate, putamen, and thalamus, as well as the hippocampus and occipital lobe) when using either the cerebellar gray matter or brainstem as reference regions. One possible explanation for the lack of significant differences in cortical amyloid- β between the two cohorts as measured by PiB PET is offered by our stereology results; the cerebellum and brainstem—both commonly used as reference regions in LOAD studies due to their relatively low PiB PET signal in LOAD cohorts—have non-trivial amyloid- β plaque burdens in the ADAD cohort. These circumstances would tend to depress regional PiB PET SUVRs in those ADAD cases with substantial cerebellar and/or brainstem amyloid- β deposits and, thus, selectively reduce the mean SUVR of the ADAD cohort, relative to that of the LOAD cohort. Importantly, this observation suggests that cerebellar gray matter and brainstem may not be appropriate reference regions for evaluating amyloid- β burden with PiB PET in many cases of ADAD. An alternative reference

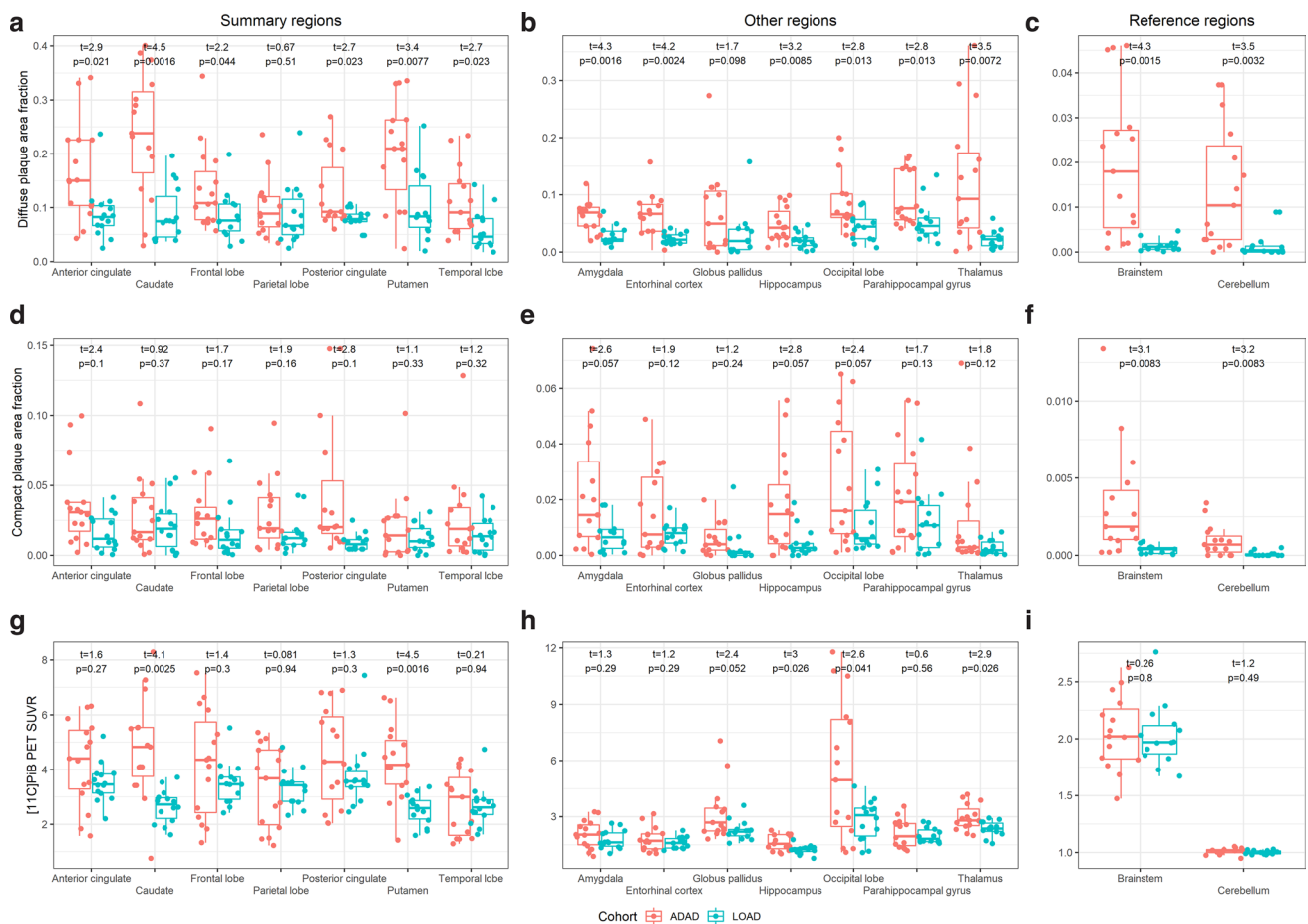


Fig. 1 Regional differences between ADAD and LOAD as measured by $[^{11}\text{C}]\text{PiB}$ PET SUVRs and plaque area fractions. Regional differences in diffuse (a–c) and compact plaque area fractions (d–f) and $[^{11}\text{C}]\text{PiB}$ PET SUVRs (g–i) across summary regions, other regions,

and reference regions between ADAD and LOAD. Differences are reported as t -values from Welch two sample t tests, accompanied by p values adjusted for FDR control by the Benjamini–Hochberg procedure

region such as the cerebellar white matter was also evaluated in this study, though using the cerebellar white matter as a reference region only showed additional significant differences in amyloid- β burden between ADAD and LOAD in the anterior cingulate, amygdala, entorhinal cortex, brainstem, cerebellum, and globus pallidus (though this last region did not demonstrate significantly different amyloid- β plaque burden in ADAD versus LOAD). Unfortunately, the previous work has shown that white matter reference regions may exhibit confounding age effects, especially in studies of LOAD [47]. Thus, comparing regional differences in amyloid- β burden accurately between ADAD and LOAD cohorts using PiB PET may be impossible using a standard approach. One compromise solution may be to use a combined cerebellar gray and white matter reference region, which mitigates the effects of amyloid- β burden in the cerebellar gray matter of ADAD individuals and potentially also the age-related changes in the cerebellar white matter of LOAD

individuals; however, this combined reference region still fails to demonstrate the elusive between-cohort differences in amyloid- β burden in several regions implicated by our stereology results (Fig. 2). Potential reasons for this discrepancy are noted in the penultimate paragraph of this Discussion.

Finally, our results suggest that diffuse and cored/compact amyloid- β plaque burdens are on average greater in ADAD than in LOAD, with diffuse plaque area fraction being greater in ADAD versus LOAD in all brain regions assessed in this study, except for the parietal lobe and globus pallidus. Interestingly, another neuropathological study showed a higher *density* of compact plaques and an equal degree of diffuse plaques in ADAD relative to LOAD, though this was a semi-quantitative study where regional distribution was not taken into account [60]. While overall amyloid- β plaque burdens may generally be greater in ADAD versus LOAD, this difference may not be true for each case of ADAD. Our current experiment encapsulates the heterogeneity in

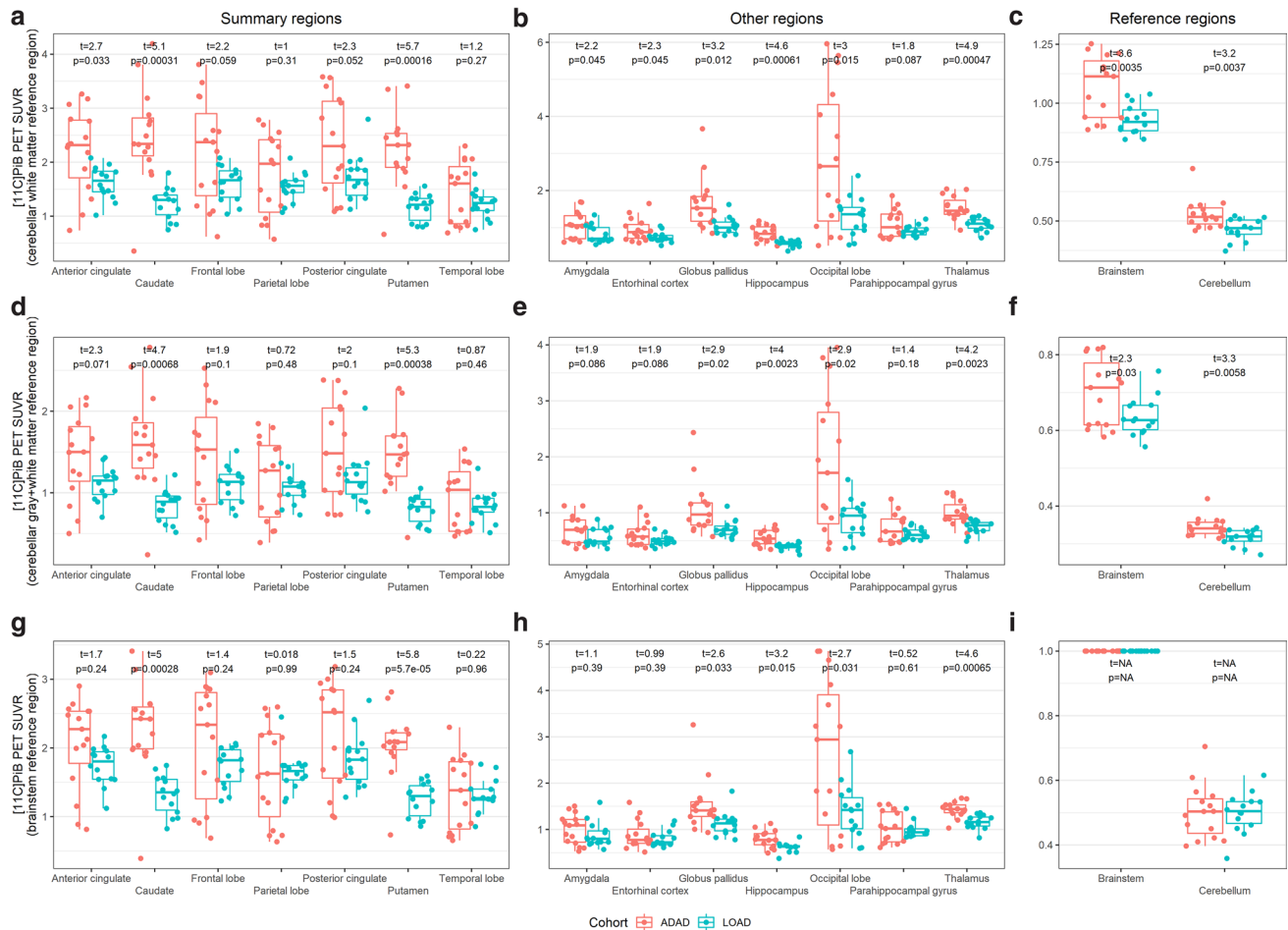


Fig. 2 Regional differences between ADAD and LOAD as measured by [11C]PiB PET SUVRs while using alternative reference regions. Regional differences in [11C]PiB PET SUVRs when using cerebellar white (a–c), cerebellar gray + white (d–f), and brainstem reference

regions (g–i) between ADAD and LOAD. Differences are reported as t -values from Welch two sample t tests, accompanied by p values adjusted for FDR control by the Benjamini–Hochberg procedure

phenotypes previously described across the amyloid- β PET imaging literature of ADAD: Koivunen and colleagues found striatal elevations in specific *PSEN1* mutation carriers [42] and Remes and colleagues found striatal and posterior cingulate elevations in *APP* mutation carriers [59]; Theuns and colleagues found an *APP* mutation carrier who demonstrated elevated amyloid- β burden in cerebral cortex with sparing of subcortex and cerebellum [74]; Tomiyama and colleagues found an *APP* mutation carrier who demonstrated very low amyloid- β signal in the brain [76], and Schöll and colleagues found a similar result in another two *APP* mutation carriers [64]. Beyond imaging studies, many other studies have observed heterogeneities in the ADAD population, including in age of onset and clinical presentation [44, 62, 65, 69] as well as implicated amyloid- β species [49, 57]. It would be of future interest to determine how the heterogeneities observed in these other domains may relate

to the heterogeneities we observed in postmortem stereology of diffuse and cored/compact plaque burden.

While general correspondence between amyloid- β PET and neuropathologic assessment has been evaluated by several studies, few have done so with unbiased, quantitative stereologic measurements as in the current study. In general, we found that the semi-quantitative ABC scoring of neuropathology cases using Thal phase, Braak NFT stage, and CERAD neuritic plaque score [28] was not granular enough to capture differences and variability between individuals and cohorts that were seen when using quantitative stereologic measurements. Notably, all ADAD cases in our study were Thal phase 5, Braak NFT stage VI, and CERAD neuritic plaque score “frequent”. Additionally, LOAD cases were mostly Thal phase 5 (with two borderline exceptions), mostly Braak NFT stage V, and all CERAD neuritic plaque score “frequent”. This is consistent with our previous study, which found substantial inter-cohort differences in tau

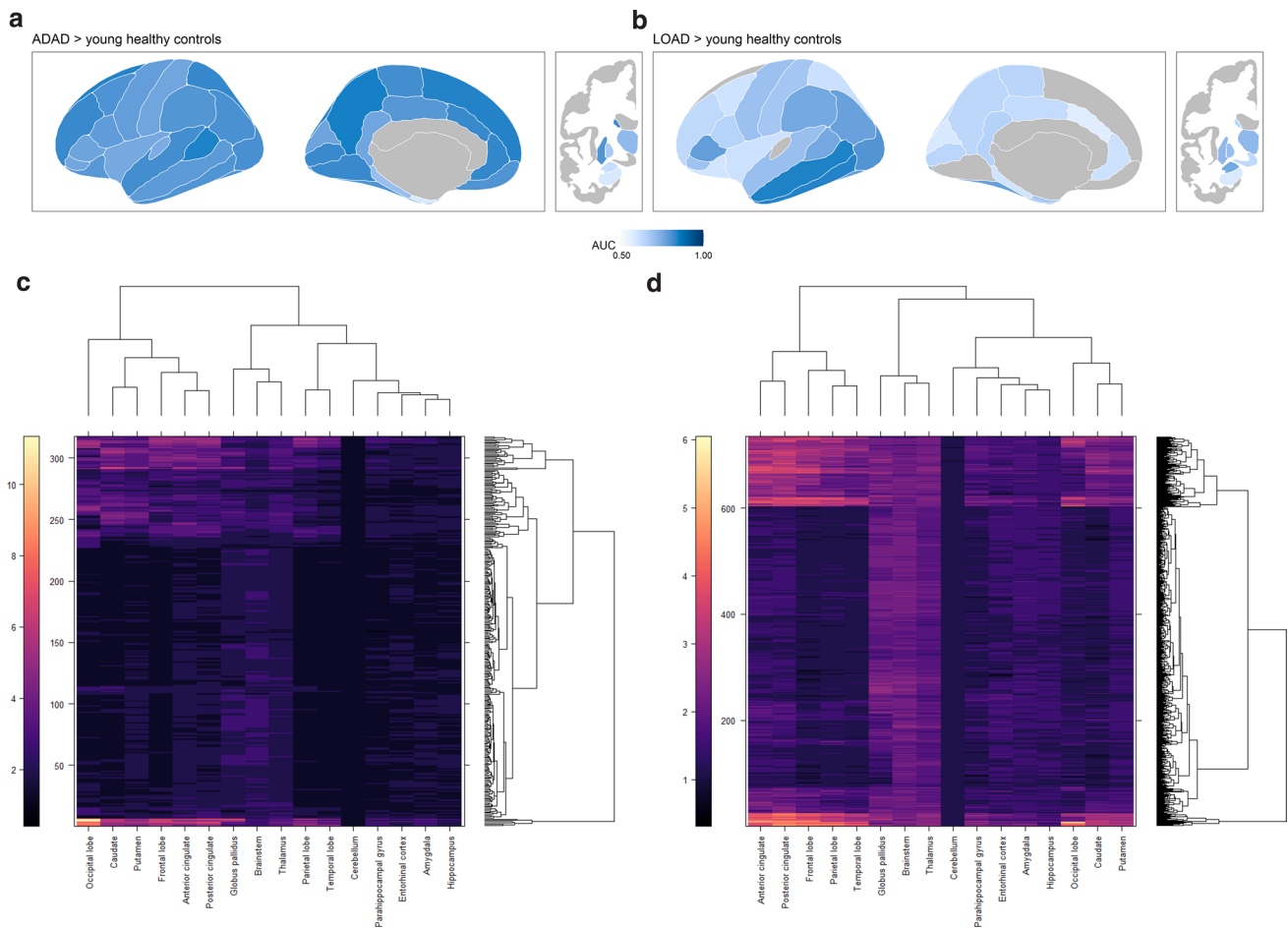


Fig. 3 Regional distributions of PiB PET SUVRs in ADAD and LOAD. Regional PiB PET SUVRs in ADAD and LOAD. **a** Regional area under the receiver-operating characteristic curves for ADAD versus young healthy controls (AUC, the probability that a randomly selected ADAD participant has a higher regional PiB PET SUVR

than a randomly selected young healthy control). **b** Regional AUCs for LOAD versus young healthy controls. **c** Heatmap and dendrograms of ADAD participants after hierarchical agglomerative clustering. **d** Heatmap and dendrograms of LOAD participants after hierarchical agglomerative clustering

neurofibrillary tangle, neuropil thread, and neuritic plaque burden in a cohort of seven ADAD and 10 LOAD individuals who were nonetheless all assessed as Braak NFT stage VI [10].

Nevertheless, several findings from previous studies are concordant with ours, even when reagents and analytic methods differ substantially. For example, Klunk and colleagues compared PiB PET SUVRs of two *PSEN1* mutation carriers who had developed clinical AD—using pons as the reference region—with qualitative assessment of 10D5-immunostained amyloid- β plaques in the striatum of the parent of one of the mutation carriers; from this indirect study, they found intense amyloid- β radiotracer binding in the striatum, consistent with findings from postmortem neuropathology [40]. Two caveats, however: first, the premise that motivated Klunk and colleagues to use the pons as a reference region—that the pons is a region free of amyloid- β —may not be true for all cases of ADAD; indeed, as our study illustrates, use

of this reference region might account for their observation that cortical amyloid- β radiotracer retention was not greater in ADAD versus LOAD. Additionally, we cannot exclude the possibility that the distribution and characteristics of amyloid- β deposits across individuals with the same pathogenic variant completely align.

Imaging-pathology correspondence has not been well studied in ADAD beyond the previous paper, but it has been more extensively studied in the LOAD literature. Clark and colleagues [12] compared semi-quantitative visual ratings and [18F]AV45 (also known as florbetapir or Amyvid) SUVRs with semi-quantitative rating and quantitative—but not stereologic—assessment of 4G8 immunostained amyloid- β plaques. This comparison was done across six regions of interest in 29 individuals (which was expanded to 59 individuals in a follow-up study [11]), ranging from cognitively normal to clinically diagnosed with LOAD and non-AD dementia, but all approaching the end-of-life [12].

In accord with the current study, Clark and colleagues found strong correlations between ante- and postmortem measurements of amyloid- β burden in the frontal, parietal, and temporal lobes and anterior cingulate gyrus, though they additionally found significant correlations in the posterior cingulate and precuneus, which did not reach significance for LOAD in our current study. That our LOAD cohort did not include cognitively normal or non-AD dementia individuals may have contributed to this difference between the two studies; other potential factors include the use of different amyloid- β PET binding agents and different primary anti-amyloid- β antibodies.

Particularly of interest are LOAD imaging-pathology studies that also use the PiB PET radioligand. Of note among these is a study by Ikonovic and colleagues, which compared PiB PET distribution volume ratios (DVRs) and quantitative—but not stereologic—assessment of 6-CN-PiB stained and 6E10 immunostained amyloid- β plaques in a single LOAD individual across 19 regions of interest, including the cortical ribbon and most subcortical nuclei, all sampled in a single axial plane; correlations were strong overall between regional PiB PET DVRs and 6E10 immunostained diffuse and cored/compact amyloid- β plaques [30]. Another study is by Driscoll and colleagues, who investigated six older adults—none of whom progressed to certain AD dementia—by comparing regional PiB PET DVRs with stereologic measurements of 6E10 immunostained amyloid- β plaques; they found statistically significant correlations in the anterior and posterior regions of the cingulate gyrus and in the precuneus [18]. Murray and colleagues investigated 35 cases with antemortem PiB PET imaging and postmortem semi-quantitative scoring and found that a PiB PET summary region SUVR of 1.4 was approximately equivalent to a Thal phase of 1–2, and that Thal phase, but not Braak NFT stage or cerebral amyloid angiopathy (CAA) score, predicted PiB PET summary region SUVRs [53]. Moving beyond PiB PET studies, Curtis and colleagues investigated 68 patients with antemortem [18F]flutemetamol PET and postmortem semi-quantitative scores; the authors found a median sensitivity and specificity of 88% among five visual readers interpreting [18F]flutemetamol PET scans as positive or negative, compared to the reference standard of postmortem neuritic plaque density as assessed by the modified CERAD score [14]. Ikonovic and colleagues studied 106 end-of-life subjects with antemortem [18F]flutemetamol PET and postmortem semi-quantitative scores, finding that the probability of an abnormal [18F]flutemetamol PET scan increased with neocortical neuritic plaque density (though diffuse plaques and CAA may explain cases with abnormal [18F]flutemetamol PET scans but low neuritic plaque burden), and concluding that amyloid- β in the form of neuritic plaques is the primary form of amyloid- β detectable by [18F]flutemetamol PET [29]. Sabri and colleagues studied

74 trial participants with antemortem [18F]florbetaben PET and postmortem CERAD scores and concluded that [18F]florbetaben PET demonstrated high sensitivity and specificity for detecting neuritic plaques [63]. Thal and colleagues investigated three cohorts of human autopsy cases neuropathologically and biochemically for the distribution of plaques and CAA, quantity, and composition of amyloid- β pathology, and found that these three measures correlated with each other and with [18F]flutemetamol PET, neurofibrillary tangles, neuritic plaques, and dementia severity [71].

One important issue to note when comparing results across studies is that not only are there differences between which amyloid- β PET radioligands are used during antemortem imaging, but there are also differences between which anti-amyloid- β antibodies are used during postmortem immunostaining. Our current study uses the 10D5 antibody to visualize amyloid- β pathology, which is an anti-amyloid- β antibody against N-terminal epitopes [19]. Antibodies against C-terminal epitopes, such as 12F4 or 4G8, may be more sensitive in detecting the earliest appearing amyloid- β deposits in AD and Down syndrome [36, 43, 45, 73], and may be of interest in future studies investigating earlier disease stages of LOAD and ADAD and making finer distinctions between plaque subtypes than in our current study.

This current study does have some additional limitations. One potential criticism of the current study is that the imaging-autopsy interval, namely the time interval between the antemortem PiB PET imaging visit and the start of autopsy, could not be matched between ADAD and LOAD cohorts. In the ADAD cohort, individuals continued to undergo PiB PET imaging exams well after showing clinical signs of AD, and imaging-autopsy intervals in the cohort ranged from 0.68 to 5.6 years with an average of 2.4 years. In contrast, individuals in the LOAD cohort did not undergo imaging studies once they progressed to moderate dementia, and the imaging-autopsy intervals ranged from 0.3 to 9.6 years with an average of 4.7 years. The primary concern would be whether this difference caused greater discordances between ante- and postmortem assessments of amyloid- β burden in the LOAD versus ADAD cohort. Relevant to this issue, two points of evidence suggest that this imaging-autopsy interval difference is not likely to account for all of the differences in amyloid burden between LOAD and ADAD. First, the strongest correlation between PiB PET SUVR and diffuse plaque burden in the entire study was observed within the LOAD cohort, within the parietal lobe (Pearson's $r=0.83$, FDR-adjusted p value = 0.00098). Second, according to highly cited leading articles in the field of AD research, amyloid- β deposition in the brain occurs over decades, and the majority of it occurs well before clinical symptoms of AD appear [32, 79]; in this scenario, a difference of 2.4 years near the end of that 15-to-20-year period is unlikely to impact amyloid burdens substantively.

Additionally, the *rate* of amyloid- β deposition slows as an individual enters the symptomatic phase of the disease, and this phenomenon lessens the effect of the imaging-autopsy interval on differences in plaque burden prior to and at death [31]. A related limitation to the long interval between PiB PET and postmortem analysis is that the AD process also advanced during this interval—the PET findings were in the milder stages of AD, whereas the postmortem analysis was at the end-stage of the disease, so end-stage findings may not reflect mild stage findings and vice versa.

Another difference between the ADAD and LOAD cohorts to be mindful is age. Age-related co-morbidities are far more common in LOAD than in ADAD [7], and three LOAD participants in this study were over 90 years of age. Specifically, in our study, we observed both microinfarcts and TDP-43 pathology, both of which are common co-morbidities among such “oldest-old” individuals [13, 55]. Nonetheless, since the focus of the current study is the quantification of amyloid- β burden, the presence of co-morbidities and their potential to contribute to dementia do not complicate our main findings. This is particularly relevant as there are no known reports of amyloid- β immunostain or radioligand off-target binding to microinfarcts or TDP-43 aggregates, which would be one way these co-morbidities could complicate the quantification of amyloid- β burden.

Another limitation of our study is the manner in which regions were matched between imaging and neuropathology. Regional PiB PET SUVRs were derived from FreeSurfer regions (from the Desikan-Killiany atlas [22]), whereas regional plaque area fractions were derived from standard tissue blocks included in DIAN and Knight ADRC postmortem assessment protocols [7]. FreeSurfer regions and tissue blocks were matched on the basis of shared nomenclature or spatial overlap; however, this solution is imperfect. One primary issue is that brain structures were segmented in their entirety through imaging, but were only be sampled in a chosen plane in neuropathology. For example, neuropathologic assessment of the hippocampus and parahippocampal gyrus was performed at the level of the lateral geniculate nucleus, whereas the hippocampus and parahippocampal gyrus were assessed in their entirety in imaging. Previous work has noted that this may lead to discordances in imaging-neuropathology comparisons [10], and future work will aim to target the same regions across both imaging and neuropathology with greater accuracy using improved co-registration methods [77].

Another limitation is that our study does not account for the presence or degree of amyloid- β deposition in the walls of small cortical blood vessels, or CAA, during stereologic quantification. CAA is known to be an additional source of the PiB PET signal [9], potentially contributing to its regional variability across disease conditions [34, 48], and can be more prevalent and severe in ADAD relative to

LOAD [60]. As such, it may account for higher PiB PET signal in the occipital lobe in ADAD versus LOAD independently of plaque burden, and otherwise influence the correlation between amyloid- β pathology and PiB PET signal in ways not measured in the current study. CAA may also impact PiB PET SUVR measurements more broadly by appearing within the cerebellum. Like the occipital lobe, the cerebellum often shows disproportionately high CAA relative to other brain areas. However, in the current study, when assessed semi-quantitatively [56, 67], CAA does not show any statistically significant correlations with diffuse or cored/compact plaque burden, or PiB PET SUVR, in either the ADAD or LOAD cohort.

We also acknowledge two other limitations of this study. The current imaging-neuropathology findings cannot address whether the PiB PET signal maintains the correlations with diffuse and compact plaque burden as seen here throughout the course of ADAD and LOAD. End-stage postmortem studies cannot determine the absolute staging of different plaque morphologies, though the earliest plaque forms observed in the non-demented aged brain are typically of the diffuse type. This observation may impact the appropriate time to administer anti-amyloid- β drug interventions, which would aim to prevent more cored/compact plaque formation; cored/compact plaques, because they are more likely to be neuritic, may be more closely linked than diffuse plaques to tau pathology, neurodegeneration, and cognitive impairment. Nonetheless, findings from our extended imaging cohort support the idea of developing separate PET staging schemes for ADAD versus LOAD across the lifespan as well. In ADAD, we see most frequent elevations of amyloid- β burden in regions outside the medial temporal lobe, while in LOAD, we see most frequent elevations of amyloid- β burden in posterolateral temporal lobe regions, suggesting two different origins of β -amyloidosis in the two diseases. Furthermore, in ADAD, striatal amyloid- β accumulation appears in step with other cortical amyloid- β accumulation, whereas in LOAD, striatal amyloid- β accumulation appears along with medial temporal lobe amyloid- β accumulation. Our observations in the ADAD participants are consistent with prior longitudinal analyses in the ADAD population [24] and our observations in the LOAD participants are consistent with prior LOAD schemes, in particular, the scheme of Grothe et al. [26], who propose that amyloid- β deposition appears first in temporobasal and frontomedial regions, and appears latest in the medial temporal lobe and striatum. Additional work is needed to understand how changes in the spatial distribution and intensity of the PiB PET signal throughout the disease course of ADAD relates to the distribution of plaque pathology, which has been more extensively studied in the context of LOAD [26, 27, 35, 70].

Finally, we note that our current histological approach measures amyloid- β plaque burden in a semi-quantitative

approach by its area. Thus, in a situation where a diffuse plaque and cored/compact plaque might have the same area, the cored/compact plaque may have a higher mass of amyloid- β . This is in contrast to the semi-quantitative nature of PiB PET, where PiB retention is proportional to the number of available binding sites—presumably determined by the mass of fibrillar amyloid- β —whether amyloid- β is deposited in the form of a diffuse or cored/compact plaque. This presumption is also somewhat speculative as it is unknown whether the PiB radiotracer can fully penetrate a solid fibrillar plaque core within the typical timeframe of a PiB PET imaging study; it is also possible that conformational and/or biochemical differences might alter the availability of binding sites. The numerous aforementioned differences in how PiB PET and amyloid- β plaques are quantified leave room for future studies to develop more comparable semi-quantitative measures of ante- and postmortem amyloid- β burden. Two promising directions are light microscope high-resolution autoradiography [8], which might be able to quantify the intensity of radiotracer signal contributed by individual plaques in a manner that avoids the issue of quantifying the mass of fibrillar amyloid- β by its area; and single-molecule imaging [17] and small angle neutron scattering [5, 75], which may help to understand the relationship between fibrillar amyloid- β aggregates and various amyloid- β plaque types. A third approach would be to move away from purely neuropathological approaches of assessing characteristics of plaque pathology to instead focus on biochemical approaches. Biochemical approaches quantifying amyloid- β species from brain tissue homogenates have shed light on amyloid pathology in LOAD, indicating increased amounts of A β 40 or A β 42(43) relative to plaque types [23, 25]. More recently, a study in LOAD evaluated biochemical fractions of amyloid- β from brain tissue compared to PET imaging to estimate which biochemical pools were most affected in AD, and derived a first approximation of the rates of amyloid- β accumulation [61]. Such approaches can also reveal distinct molecular profiles of amyloid- β in LOAD and ADAD [21].

In summary, our data indicate that there is a close association between fibrillar amyloid- β burdens as visualized by PiB PET and as assessed by postmortem stereologic measures. Caveats may be raised: individuals with ADAD show considerable variability in amyloid- β burden and distribution that can also differ considerably from that typical of LOAD; therefore, summary and reference regions commonly used in PiB PET studies of LOAD may potentially need to be adjusted for PiB PET studies of ADAD. This point is especially important when evaluating anti-amyloid- β drug trials that enroll participants with ADAD. In such studies, investigators should be alert to the possibility of variable drug responses and interpret differences in cross-sectional measures of amyloid- β burden between treatment groups with

care; indeed, individual-focused longitudinal monitoring strategies might be favorable. Additionally, when comparing trials of the same anti-amyloid- β drug conducted in ADAD versus LOAD, investigators should note that the choice of reference region can strongly influence interpretations of regional amyloid- β burden differences between cohorts.

Supplementary Information The online version contains supplementary material available at <https://doi.org/10.1007/s00401-021-02342-y>.

Funding Data collection and sharing for this project was supported by the Knight Alzheimer Disease Research Center (Knight ADRC, P30AG066444, P01AG026276, and P01AG03991) and the Dominantly Inherited Alzheimer Network (DIAN, U19AG032438). This manuscript has been reviewed by DIAN Study investigators for scientific content and consistency of data interpretation with previous DIAN Study publications. We acknowledge the altruism of the participants and their families and contributions of the Knight ADRC and DIAN research and support staff at each of the participating sites for their contributions to this study. For the provision of brain tissue and staining, we acknowledge the Knight ADRC Neuropathology Core and the DIAN Neuropathology Core (P01AG003991). We thank the staff of the Betty Martz Laboratory for Neurodegenerative Disease for their excellent technical support. The authors also acknowledge support from the Neuroimaging Informatics and Analysis Center (P30NS098577). C.D.C. acknowledges support from the NSF GRFP (DGE-1745038). N.J.M. acknowledges support from the Alzheimer's Association International Research Grant Program (AARFD-20-681815). B.A.G. acknowledges support from the NIH (K01AG053474). J.C.M. acknowledges support from the NIH (U19AG032438).

Declarations

Conflict of interest J.C. has served on a medical advisory board for Otsuka Pharmaceuticals. GE Healthcare holds a license agreement with the University of Pittsburgh based on the PiB-PET technology described in this manuscript. W.E.K. is a co-inventor of PiB and, as such, has a financial interest in this license agreement. GE Healthcare provided no grant support for this study and had no role in the design or interpretation of results or preparation of this manuscript. All other authors have no conflicts of interest with PiB-PET and had full access to all of the data in the study and take responsibility for the integrity of the data and the accuracy of the data analysis. J.C.M. is funded by NIH grants # P30 AG066444; P01AG003991; P01AG026276; U19 AG032438; and U19 AG024904. Neither J.C.M. nor his family owns stock or has equity interest (outside of mutual funds or other externally directed accounts) in any pharmaceutical or biotechnology company. T.L.S.B. has investigator-initiated research funding from the NIH, the Alzheimer's Association, the Barnes-Jewish Hospital Foundation, and Avid Radiopharmaceuticals (a wholly owned subsidiary of Eli Lilly); participates as a site investigator in clinical trials sponsored by Avid Radiopharmaceuticals, Eli Lilly, Biogen, Eisai, Jaansen, and Roche; serves as an unpaid consultant to Eisai and Siemens; and is on the Speaker's Bureau for Biogen.

Data and materials availability Data are available by request to the Knight ADRC (knightadrc.wustl.edu/research/resourcerequest.htm) and the DIAN-Obs (dian.wustl.edu/our-research/observational-study/dian-observational-study-investigator-resources/data-request-terms-and-instructions/).

References

- Bateman RJ, Aisen PS, De Strooper B, Fox NC, Lemere CA, Ringman JM et al (2011) Autosomal-dominant Alzheimer's disease: a review and proposal for the prevention of Alzheimer's disease. *Alz Res Therapy* 3, 1. <https://doi.org/10.1186/alzrt59>
- Benzinger TLS, Blazey T, Jack CR, Koeppe RA, Su Y, Xiong C et al (2013) Regional variability of imaging biomarkers in autosomal dominant Alzheimer's disease. *Proc Natl Acad Sci USA* 110:E4502–E4509. <https://doi.org/10.1073/pnas.1317918110>
- Van Berckel BNM, Ossenkoppele R, Tolboom N, Yaqub M, Foster-Dingley JC, Windhorst AD et al (2013) Longitudinal amyloid imaging using 11C-PiB: Methodologic considerations. *J Nucl Med* 54:1570–1576. <https://doi.org/10.2967/jnumed.112.113654>
- Braak H, Braak E (1991) Neuropathological staging of Alzheimer-related changes. *Acta Neuropathol* 82:239–259. <https://doi.org/10.1007/BF00308809>
- Burkoth TS, Benzinger TLS, Urban V, Lynn DG, Meredith SC, Thiyagarajan P (1999) Self-assembly of A β ((10–35))-PEG block copolymer fibrils [13]. *J Am Chem Soc* 121:7429–7430
- van Buuren S, Groothuis-Oudshoorn K (2011) Mice: multivariate imputation by chained equations in R. *J Stat Softw* 45:1–67. <https://doi.org/10.18637/jss.v045.i03>
- Cairns NJ, Perrin RJ, Franklin EE, Carter D, Vincent B, Xie M et al (2015) Neuropathologic assessment of participants in two multi-center longitudinal observational studies: the Alzheimer Disease Neuroimaging Initiative (ADNI) and the Dominantly Inherited Alzheimer Network (DIAN). *Neuropathology* 35:390–400. <https://doi.org/10.1111/neup.12205>
- Caro LG (1964) Chapter 16 high-resolution autoradiography. *Methods Cell Biol* 1:327–363. [https://doi.org/10.1016/S0091-679X\(08\)62098-1](https://doi.org/10.1016/S0091-679X(08)62098-1)
- Charidimou A, Farid K, Baron JC (2017) Amyloid-PET in sporadic cerebral amyloid angiopathy. *Neurology* 89:1490–1498. <https://doi.org/10.1212/WNL.0000000000004539>
- Chen CD, Holden TR, Gordon BA, Franklin EE, Li Y, Coble DW et al (2020) Ante- and postmortem tau in autosomal dominant and late-onset Alzheimer's disease. *Ann Clin Transl Neurol* 7:2475–2480. <https://doi.org/10.1002/acn3.51237>
- Clark CM, Pontecorvo MJ, Beach TG, Bedell BJ, Coleman RE, Doraiswamy PM et al (2012) Cerebral PET with florbetapir compared with neuropathology at autopsy for detection of neuritic amyloid- β plaques: a prospective cohort study. *Lancet Neurol* 11:669–678. [https://doi.org/10.1016/S1474-4422\(12\)70142-4](https://doi.org/10.1016/S1474-4422(12)70142-4)
- Clark CM, Schneider JA, Bedell BJ, Beach TG, Bilker WB, Mintun MA et al (2011) Use of Florbetapir-PET for imaging β -amyloid pathology. *JAMA* 305(3):275–283. <https://doi.org/10.1001/JAMA.2010.2008>
- Corrada MM, Sonnen JA, Kim RC, Kawas CH (2016) Microinfarcts are common and strongly related to dementia in the oldest-old: The 90+ study. *Alzheimer's Dement* 12:900–908. <https://doi.org/10.1016/j.jalz.2016.04.006>
- Curtis C, Gamez JE, Singh U, Sadowsky CH, Villena T, Sabbagh MN et al (2015) Phase 3 trial of flutemetamol labeled with radioactive fluorine 18 imaging and neuritic plaque density. *JAMA Neurol* 72:287–294. <https://doi.org/10.1001/jamaneurol.2014.4144>
- Davies CA, Mann DMA (1993) Is the "preamyloid" of diffuse plaques in Alzheimer's disease really nonfibrillar? *Am J Pathol* 143:1594–1605
- Dickson TC, Vickers JC (2001) The morphological phenotype of β -amyloid plaques and associated neuritic changes in Alzheimer's disease. *Neuroscience* 105:99–107. [https://doi.org/10.1016/S0306-4522\(01\)00169-5](https://doi.org/10.1016/S0306-4522(01)00169-5)
- Ding T, Wu T, Mazidi H, Zhang O, Lew MD (2020) Single-molecule orientation localization microscopy for resolving structural heterogeneities between amyloid fibrils. *Optica* 7:602. <https://doi.org/10.1364/optica.388157>
- Driscoll I, Troncoso JC, Rudow G, Sojkova J, Pletnikova O, Zhou Y et al (2012) Correspondence between in vivo 11C-PiB-PET amyloid imaging and postmortem, region-matched assessment of plaques. *Acta Neuropathol* 124:823–831. <https://doi.org/10.1007/s00401-012-1025-1>
- Dé Rique Bard F, Barbour R, Cannon C, Carretto R, Fox M, Games D et al (2003) Epitope and isotype specificities of antibodies to-amyloid peptide for protection against Alzheimer's disease-like neuropathology. *Proceedings of the National Academy of Sciences* 100(4):2023–2028. <https://doi.org/10.1073/pnas.0436286100>
- Efron B (2007) Size, power and false discovery rates. *Ann Stat* 35:1351–1377. <https://doi.org/10.1214/009053606000001460>
- Di Fede G, Catania M, Maderna E, Ghidoni R, Benussi L, Tonoli E et al (2018) Molecular subtypes of Alzheimer's disease. *Sci Rep*. <https://doi.org/10.1038/s41598-018-21641-1>
- Fischl B, Salat DH, Busa E, Albert M, Dieterich M, Haselgrove C et al (2002) Whole brain segmentation: automated labeling of neuroanatomical structures in the human brain. *Neuron* 33:341–355. [https://doi.org/10.1016/S0896-6273\(02\)00569-X](https://doi.org/10.1016/S0896-6273(02)00569-X)
- Frucht SJ, Koo EH (1993) β -amyloid protein is higher in Alzheimer's disease brains: description of a quantitative biochemical assay. *J Neuropathol Exp Neurol* 52:640–647. <https://doi.org/10.1097/00005072-199311000-00011>
- Gordon BA, Blazey TM, Su Y, Hari-Raj A, Dincer A, Flores S et al (2018) Spatial patterns of neuroimaging biomarker change in individuals from families with autosomal dominant Alzheimer's disease: a longitudinal study. *Lancet Neurol* 17:241–250. [https://doi.org/10.1016/S1474-4422\(18\)30028-0](https://doi.org/10.1016/S1474-4422(18)30028-0)
- Gravina SA, Ho L, Eckman CB, Long KE, Otvos L, Younkin LH et al (1995) Amyloid β protein (A β) in Alzheimer's disease brain. Biochemical and immunocytochemical analysis with antibodies specific for forms ending at A β 40 or A β 42(43). *J Biol Chem* 270:7013–7016. <https://doi.org/10.1074/jbc.270.13.7013>
- Grothe MJ, Barthel H, Sepulcre J, Dyrba M, Sabri O, Teipel SJ (2017) In vivo staging of regional amyloid deposition. *Neurology* 89:2031–2038. <https://doi.org/10.1212/WNL.0000000000004643>
- Hanseeuw BJ, Betensky RA, Mormino EC, Schultz AP, Sepulcre J, Becker JA et al (2018) PET staging of amyloidosis using striatum. *Alzheimer's Dement* 14:1281–1292. <https://doi.org/10.1016/j.jalz.2018.04.011>
- Hyman BT, Phelps CH, Beach TG, Bigio EH, Cairns NJ, Carrillo MC et al (2012) National Institute on Aging-Alzheimer's Association guidelines for the neuropathologic assessment of Alzheimer's disease. *Alzheimer's Dement* 8:1–13. <https://doi.org/10.1016/j.jalz.2011.10.007>
- Ikonomic MD, Buckley CJ, Heurling K, Sherwin P, Jones PA, Zanette M et al (2016) Post-mortem histopathology underlying β -amyloid PET imaging following flutemetamol F 18 injection. *Acta Neuropathol Commun* 4:130. <https://doi.org/10.1186/s40478-016-0399-z>
- Ikonomic MD, Klunk WE, Abrahamson EE, Mathis CA, Price JC, Tsopoulos ND et al (2008) Post-mortem correlates of in vivo PiB-PET amyloid imaging in a typical case of Alzheimer's disease. *Brain* 131:1630–1645. <https://doi.org/10.1093/brain/awn016>
- Jack CR, Knopman DS, Jagust WJ, Petersen RC, Weiner MW, Aisen PS et al (2013) Tracking pathophysiological processes in Alzheimer's disease: an updated hypothetical model of dynamic biomarkers. *Lancet Neurol* 12:207–216
- Jack CR, Knopman DS, Jagust WJ, Shaw LM, Aisen PS, Weiner MW et al (2010) Hypothetical model of dynamic biomarkers of the Alzheimer's pathological cascade. *Lancet Neurol* 9:119–128

33. James G, Witten D, Hastie T, Tibshirani R (2017) An introduction to statistical learning. Springer, New York
34. Johnson KA, Gregas M, Becker JA, Kinnecom C, Salat DH, Moran EK et al (2007) Imaging of amyloid burden and distribution in cerebral amyloid angiopathy. *Ann Neurol* 62:229–234. <https://doi.org/10.1002/ana.21164>
35. La Joie R, Ayakta N, Seeley WW, Borys E, Boxer AL, DeCarli C et al (2019) Multisite study of the relationships between antemortem [11 C]PIB-PET Centiloid values and postmortem measures of Alzheimer's disease neuropathology. *Alzheimer's Dement* 15:205–216. <https://doi.org/10.1016/j.jalz.2018.09.001>
36. Kida E, Wisniewski KE, Wisniewski HM (1995) Early amyloid- β deposits show different immunoreactivity to the amino- and carboxy-terminal regions of β -peptide in Alzheimer's disease and Down's syndrome brain. *Neurosci Lett* 193:105–108. [https://doi.org/10.1016/0304-3940\(95\)11678-P](https://doi.org/10.1016/0304-3940(95)11678-P)
37. Klunk WE, Engler H, Nordberg A, Wang Y, Blomqvist G, Holt DP et al (2004) Imaging brain amyloid in Alzheimer's Disease with Pittsburgh Compound-B. *Ann Neurol* 55:306–319. <https://doi.org/10.1002/ana.20009>
38. Klunk WE, Koeppe RA, Price JC, Benzinger TL, Devous MD, Jagust WJ et al (2015) The Centiloid project: standardizing quantitative amyloid plaque estimation by PET. *Alzheimer's Dement* 11:1-15.e4. <https://doi.org/10.1016/j.jalz.2014.07.003>
39. Klunk WE, Lopresti BJ, Ikonovic MD, Lefterov IM, Koldamova RP, Abrahamson EE et al (2005) Binding of the positron emission tomography tracer Pittsburgh Compound-B reflects the amount of amyloid- β in Alzheimer's Disease brain but not in transgenic mouse brain. *J Neurosci* 25:10598–10606. <https://doi.org/10.1523/JNEUROSCI.2990-05.2005>
40. Klunk WE, Price JC, Mathis CA, Tsopelas ND, Lopresti BJ, Ziolko SK et al (2007) Amyloid deposition begins in the striatum of presenilin-1 mutation carriers from two unrelated pedigrees. *J Neurosci* 27:6174–6184. <https://doi.org/10.1523/JNEUROSCI.0730-07.2007>
41. Knowles RB, Wyart C, Buldyrev SV, Cruz L, Urbanc B, Hasselmo ME et al (1999) Plaque-induced neurite abnormalities: implications for disruption of neural networks in Alzheimer's disease. *Proc Natl Acad Sci USA* 96:5274–5279. <https://doi.org/10.1073/pnas.96.9.5274>
42. Koivunen J, Verkkoniemi A, Aalto S, Paetau A, Ahonen JP, Viitanen M et al (2008) PET amyloid ligand [11C]PIB uptake shows predominantly striatal increase in variant Alzheimer's disease. *Brain* 131:1845–1853. <https://doi.org/10.1093/brain/awn107>
43. Lalowski M, Golabek A, Lemere CA, Selkoe DJ, Wisniewski HM, Beavis RC et al (1996) The "Nonamyloidogenic" p3 fragment (amyloid β 17-42) is a major constituent of down's syndrome cerebellar preamyloid. *J Biol Chem* 271:33623–33631. <https://doi.org/10.1074/jbc.271.52.33623>
44. Larner AJ, Doran M (2006) Clinical phenotypic heterogeneity of Alzheimer's disease associated with mutations of the presenilin-1 gene. *J Neurol* 253:139–158
45. Lemere CA, Blusztajn JK, Yamaguchi H, Wisniewski T, Saido TC, Selkoe DJ (1996) Sequence of deposition of heterogeneous amyloid β -peptides and APO E in down syndrome: implications for initial events in amyloid plaque formation. *Neurobiol Dis* 3:16–32. <https://doi.org/10.1006/nbdi.1996.0003>
46. Lockhart A, Lamb JR, Osredkar T, Sue LI, Joyce JN, Ye L et al (2007) PIB is a non-specific imaging marker of amyloid-beta (A β) peptide-related cerebral amyloidosis. *Brain* 130:2607–2615. <https://doi.org/10.1093/brain/awn191>
47. Lowe VJ, Lundt ES, Senjem ML, Schwarz CG, Min HK, Przybelski SA et al (2018) White matter reference region in PET studies of 11C-Pittsburgh compound B uptake: effects of age and amyloid- β deposition. *J Nucl Med* 59:1583–1589. <https://doi.org/10.2967/jnumed.117.204271>
48. Ly JV, Donnan GA, Villemagne VL, Zavala JA, Ma H, O'Keefe G et al (2010) 11C-PIB binding is increased in patients with cerebral amyloid angiopathy-related hemorrhage. *Neurology* 74:487–493. <https://doi.org/10.1212/WNL.0b013e3181cef7e3>
49. Maarouf CL, Dausgs ID, Spina S, Vidal R, Kokjohn TA, Patton RL et al (2008) Histopathological and molecular heterogeneity among individuals with dementia associated with Presenilin mutations. *Mol Neurodegener* 3:20. <https://doi.org/10.1186/1750-1326-3-20>
50. Mirra SS, Heyman A, McKeel D, Sumi SM, Crain BJ, Brownlee LM et al (1991) The consortium to establish a registry for Alzheimer's disease (CERAD). Part II. Standardization of the neuropathologic assessment of Alzheimer's disease. *Neurology* 41:479–486. <https://doi.org/10.1212/wnl.41.4.479>
51. Montine TJ, Phelps CH, Beach TG, Bigio EH, Cairns NJ, Dickson DW et al (2012) National institute on aging-Alzheimer's association guidelines for the neuropathologic assessment of Alzheimer's disease: a practical approach. *Acta Neuropathol* 123:1–11. <https://doi.org/10.1007/s00401-011-0910-3>
52. Morris JC, Aisen PS, Bateman RJ, Benzinger TL, Cairns NJ, Fagan AM et al (2012) Developing an international network for Alzheimer's research: the dominantly inherited alzheimer network. *Clin Investig (Lond)* 2:975–984. <https://doi.org/10.4155/cli.12.93>
53. Murray ME, Lowe VJ, Graff-Radford NR, Liesinger AM, Cannon A, Przybelski SA et al (2015) Clinicopathologic and 11C-Pittsburgh compound B implications of Thal amyloid phase across the Alzheimer's disease spectrum. *Brain* 138:1370–1381. <https://doi.org/10.1093/brain/awv050>
54. Nelson PT, Alafuzoff I, Bigio EH, Bouras C, Braak H, Cairns NJ et al (2012) Correlation of Alzheimer disease neuropathologic changes with cognitive status: a review of the literature. *J Neuropathol Exp Neurol* 71:362–381
55. Nelson PT, Dickson DW, Trojanowski JQ, Jack CR, Boyle PA, Arfanakis K et al (2019) Limbic-predominant age-related TDP-43 encephalopathy (LATE): consensus working group report. *Brain* 142:1503–1527
56. Olichney JM, Hansen LA, Hofstetter CR, Lee JH, Katzman R, Thal LJ (2000) Association between severe cerebral amyloid angiopathy and cerebrovascular lesions in Alzheimer disease is not a spurious one attributable to apolipoprotein E4. *Arch Neurol* 57:869–874. <https://doi.org/10.1001/archneur.57.6.869>
57. Portelius E, Andreasson U, Ringman JM, Buerger K, Daborg J, Buchhave P et al (2010) Distinct cerebrospinal fluid amyloid peptide signatures in sporadic and PSEN1 A431E-associated familial Alzheimer's disease. *Mol Neurodegener* 5:2. <https://doi.org/10.1186/1750-1326-5-2>
58. Price JL, McKeel DW, Buckles VD, Roe CM, Xiong C, Grundman M et al (2009) Neuropathology of nondemented aging: presumptive evidence for preclinical Alzheimer disease. *Neurobiol Aging* 30:1026–1036. <https://doi.org/10.1016/j.neurobiolaging.2009.04.002>
59. Remes AM, Laru L, Tuominen H, Aalto S, Kempainen N, Mononen H et al (2008) Carbon 11-labeled Pittsburgh Compound B positron emission tomographic amyloid imaging in patients with APP locus duplication. *Arch Neurol* 65:540–544. <https://doi.org/10.1001/archneur.65.4.540>
60. Ringman JM, Monsell S, Ng DW, Zhou Y, Nguyen A, Coppola G et al (2016) Neuropathology of autosomal dominant Alzheimer disease in the National Alzheimer Coordinating Center Database. *J Neuropathol Exp Neurol* 75:284. <https://doi.org/10.1093/JNEN/NLV028>
61. Roberts BR, Lind M, Wagen AZ, Rembach A, Frugier T, Li QX et al (2017) Biochemically-defined pools of amyloid- β in sporadic Alzheimer's disease: Correlation with amyloid PET. *Brain* 140:1486–1498. <https://doi.org/10.1093/brain/awx057>

62. Ryman DC, Acosta-Baena N, Aisen PS, Bird T, Danek A, Fox NC et al (2014) Symptom onset in autosomal dominant Alzheimer disease: a systematic review and meta-analysis. *Neurology* 83:253–260. <https://doi.org/10.1212/WNL.0000000000000596>
63. Sabri O, Sabbagh MN, Seibyl J, Barthel H, Akatsu H, Ouchi Y et al (2015) Florbetaben PET imaging to detect amyloid beta plaques in Alzheimer's disease: Phase 3 study. *Alzheimer's Dement* 11:964–974. <https://doi.org/10.1016/j.jalz.2015.02.004>
64. Schöll M, Wall A, Thordardottir S, Ferreira D, Bogdanovic N, Långström B et al (2012) Low PiB PET retention in presence of pathologic CSF biomarkers in Arctic APP mutation carriers. *Neurology* 79:229–236. <https://doi.org/10.1212/WNL.0b013e31825fdf18>
65. Sepulveda-Falla D, Chavez-Gutierrez L, Portelius E, Vézé JI, Barrera-Ocampo A, Dinkel F et al (2018) A multifactorial model of pathology for age of onset variability in Familial Alzheimer's disease. *Sci Transl Med* revised ver. <https://doi.org/10.1007/s00401-020-02249-0>
66. Su Y, Blazey TM, Snyder AZ, Raichle ME, Marcus DS, Ances BM et al (2015) Partial volume correction in quantitative amyloid imaging. *Neuroimage* 107:55–64. <https://doi.org/10.1016/j.neuroimage.2014.11.058>
67. Su Y, D'Angelo GM, Vlassenko AG, Zhou G, Snyder AZ, Marcus DS et al (2013) Quantitative analysis of PiB-PET with FreeSurfer ROIs. *PLoS ONE* 8:e73377. <https://doi.org/10.1371/journal.pone.0073377>
68. Su Y, Flores S, Hornbeck RC, Speidel B, Vlassenko AG, Gordon BA et al (2018) Utilizing the Centiloid scale in cross-sectional and longitudinal PiB PET studies. *NeuroImage Clin* 19:406–416. <https://doi.org/10.1016/j.nicl.2018.04.022>
69. Tang M, Ryman DC, McDade E, Jasielec MS, Buckles VD, Cairns NJ et al (2016) Neurological manifestations of autosomal dominant familial Alzheimer's disease: a comparison of the published literature with the Dominantly Inherited Alzheimer Network observational study (DIAN-OBS). *Lancet Neurol* 15:1317–1325. [https://doi.org/10.1016/S1474-4422\(16\)30229-0](https://doi.org/10.1016/S1474-4422(16)30229-0)
70. Thal DR, Beach TG, Zanette M, Lilja J, Heurling K, Chakrabarty A et al (2018) Estimation of amyloid distribution by [18F] flutemetamol PET predicts the neuropathological phase of amyloid β -protein deposition. *Acta Neuropathol* 136:557–567. <https://doi.org/10.1007/s00401-018-1897-9>
71. Thal DR, Ronisz A, Tousseyn T, Rijal Upadhaya A, Balakrishnan K, Vandenberghe R et al (2019) Different aspects of Alzheimer's disease-related amyloid β -peptide pathology and their relationship to amyloid positron emission tomography imaging and dementia. *Acta Neuropathol Commun* 7:178. <https://doi.org/10.1186/s40478-019-0837-9>
72. Thal DR, Rüb U, Orantes M, Braak H (2002) Phases of A β -deposition in the human brain and its relevance for the development of AD. *Neurology* 58:1791–1800. <https://doi.org/10.1212/WNL.58.12.1791>
73. Thal DR, Sassin I, Schultz C, Haass C, Braak E, Braak H (1999) Fleecy amyloid deposits in the internal layers of the human entorhinal cortex are comprised of N-terminal truncated fragments of A β . *J Neuropathol Exp Neurol* 58:210–216. <https://doi.org/10.1097/00005072-199902000-00010>
74. Theuns J, Marjaux E, Vandenbulcke M, Van Laere K, Kumar-Singh S, Bormans G et al (2006) Alzheimer dementia caused by a novel mutation located in the APP C-terminal intracytosolic fragment. *Hum Mutat* 27:888–896. <https://doi.org/10.1002/humu.20402>
75. Thiyagarajan P, Burkoth TS, Urban V, Seifert S, Benzinger TLS, Morgan DM et al (2000) pH dependent self assembly of β -amyloid(10–35) and β -amyloid(10–35)-PEG3000. *J Appl Cryst* 33:535–539. <https://doi.org/10.1107/S0021889899014387>
76. Tomiyama T, Nagata T, Shimada H, Teraoka R, Fukushima A, Kanemitsu H et al (2008) A new amyloid β variant favoring oligomerization in Alzheimer's-type dementia. *Ann Neurol* 63:377–387. <https://doi.org/10.1002/ana.21321>
77. Van Essen DC, Jbabdi S, Sotiropoulos SN, Chen C, Dikranian K, Coalson T et al (2013) Mapping connections in humans and non-human primates: aspirations and challenges for diffusion imaging. In: *Diffusion MRI: from quantitative measurement to in vivo neuroanatomy*, 2nd edn. Elsevier Inc., Amsterdam, pp 337–358. <https://doi.org/10.1016/B978-0-12-396460-1.00016-0>
78. Verwey NA, Hoozemans JJM, Korth C, Van Royen MR, Prikulis I, Wouters D et al (2013) Immunohistochemical characterization of novel monoclonal antibodies against the N-terminus of amyloid β -peptide. *Amyloid* 20:179–187. <https://doi.org/10.3109/13506129.2013.797389>
79. Villemagne VL, Burnham S, Bourgeat P, Brown B, Ellis KA, Salvado O et al (2013) Amyloid β deposition, neurodegeneration, and cognitive decline in sporadic Alzheimer's disease: a prospective cohort study. *Lancet Neurol* 12:357–367. [https://doi.org/10.1016/S1474-4422\(13\)70044-9](https://doi.org/10.1016/S1474-4422(13)70044-9)
80. Vonsattel JPG, Myers RH, Tessa Hedley-Whyte E, Ropper AH, Bird ED, Richardson EP (1991) Cerebral amyloid angiopathy without and with cerebral hemorrhages: a comparative histological study. *Ann Neurol* 30:637–649. <https://doi.org/10.1002/ana.410300503>
81. Wong DF, Rosenberg PB, Zhou Y, Kumar A, Raymond V, Ravert HT et al (2010) In vivo imaging of amyloid deposition in Alzheimer disease using the radioligand 18F-AV-45 (florbetapir F 18). *J Nucl Med* 51:913–920. <https://doi.org/10.2967/jnumed.109.069088>

Publisher's Note Springer Nature remains neutral with regard to jurisdictional claims in published maps and institutional affiliations.

Authors and Affiliations

Charles D. Chen¹ · Nelly Joseph-Mathurin¹ · Namita Sinha^{2,3} · Aihong Zhou⁴ · Yan Li⁵ · Karl Friedrichsen⁶ · Austin McCullough¹ · Erin E. Franklin² · Russ Hornbeck¹ · Brian Gordon¹ · Vijay Sharma¹ · Carlos Cruchaga⁷ · Alison Goate⁸ · Celeste Karch⁷ · Eric McDade⁵ · Chengjie Xiong⁵ · Randall J. Bateman⁵ · Bernardino Ghetti⁹ · John M. Ringman¹⁰ · Jasmeer Chhatwal¹¹ · Colin L. Masters¹² · Catriona McLean¹³ · Tammarny Lashley^{14,15} · Yi Su^{16,17} · Robert Koeppe¹⁸ · Clifford Jack¹⁹ · William E. Klunk²⁰ · John C. Morris⁵ · Richard J. Perrin^{2,5} · Nigel J. Cairns^{2,5,21} · Tammie L. S. Benzinger¹

- ¹ Mallinckrodt Institute of Radiology, Washington University in St. Louis, St. Louis, MO, USA
- ² Department of Pathology and Immunology, Washington University in St. Louis, St. Louis, MO, USA
- ³ Department of Pathology, University of Manitoba, Shared Health, Winnipeg, MB, Canada
- ⁴ Department of Neurology, Xuanwu Hospital, Capital Medical University, Beijing, China
- ⁵ Department of Neurology, Washington University in St. Louis, St. Louis, MO, USA
- ⁶ Department of Ophthalmology and Visual Sciences, Washington University in St. Louis, St. Louis, MO, USA
- ⁷ Department of Psychiatry, Washington University in St. Louis, St. Louis, MO, USA
- ⁸ Department of Genetics and Genomic Sciences, Ichan School of Medicine at Mount Sinai, New York, NY, USA
- ⁹ Department of Pathology and Laboratory Medicine, Indiana University School of Medicine, Indianapolis, IN, USA
- ¹⁰ Department of Neurology, Keck School of Medicine of USC, Los Angeles, CA, USA
- ¹¹ Department of Neurology, Massachusetts General Hospital, Harvard Medical School, Boston, MA, USA
- ¹² The Florey Institute of Neuroscience and Mental Health, The University of Melbourne, Melbourne, VIC, Australia
- ¹³ Department of Anatomic Pathology, Alfred Hospital, Melbourne, VIC, Australia
- ¹⁴ UCL Queen Square Institute of Neurology, University College London, London, UK
- ¹⁵ Queen Square Brain Bank for Neurological Disorders, University College London, London, UK
- ¹⁶ Banner Alzheimer's Institute, Banner Health, Phoenix, AZ, USA
- ¹⁷ Arizona Alzheimer's Consortium, Banner Health, Phoenix, AZ, USA
- ¹⁸ Department of Radiology, University of Michigan, Ann Arbor, MI, USA
- ¹⁹ Department of Radiology, Mayo Clinic, Rochester, MN, USA
- ²⁰ Department of Psychiatry, University of Pittsburgh, Pittsburgh, PA, USA
- ²¹ College of Medicine and Health, University of Exeter, Exeter, UK